Novel Solanum torvum Fruit Biomass-Derived Hierarchical Porous Carbon Nanosphere as Excellent Electrode Material for Enhanced Symmetric Supercapacitor Performance

by Rika Taslim

Submission date: 29-Apr-2023 06:10PM (UTC+0700)
Submission ID: 2079115882
File name: s11837-023-05801-x.pdf (2.06M)
Word count: 8340
Character count: 42436

JOM
https://doi.org/10.1007/s11837-023-05801-x

Novel *Solanum torvum* Fruit Biomass-Derived Hierarchical Porous Carbon Nanosphere as Excellent Electrode Material for Enhanced Symmetric Supercapacitor Performance

ERMAN TAER,[1] NURSYAFNI SYAMSUNAR,[1] APRIWANDI APRIWANDI,[1] and RIKA TASLIM [2,3]

1.—Department of Physics, Faculty of Mathematic and Natural Sciences, University of Riau, Pekanbaru 28293, Indonesia. 2.—Department of Industrial Engineering, State Islamic University Sultan Syarif Kasim Riau, Pekanbaru 28293, Indonesia. 3.—e-mail: rikataslim@gmail.com

Biomass-based hierarchical porous carbon nanospheres offer an outstanding performance of electrode materials in electrochemical energy storage device applications. However, integrating all these advantages into one fabric is still a challenge. Therefore, this study aims to develop novel biomass of *Solanum torvum* fruit (STF) as a hierarchical porous carbon nanosphere source for high-quality electrode material for supercapacitor applications. The STF-based carbon nanospheres were synthesized with a green, sustainable strategy through $ZnCl_2$ impregnation, carbonization, and physical activation. Through the 0.5 M $ZnCl_2$, it was discovered that the carbon nanosphere maintains a dense spherical structure with enriched 3D "cow tripe-like" hierarchical pores. The optimized carbon nanosphere yielded a high specific surface area of 1176.29 m^2g^{-1} with a nearly balanced combination of the micro-mesopores. The combination of the 3D hierarchical pore structure and densely packed nanospheres gave high electrochemical properties of the symmetric supercapacitor with a delightful specific capacitance of 154 Fg^{-1} at 1 Ag^{-1} in the H_2SO_4 electrolyte and high cyclic performance with coulombic efficiency ~ 84.5%. The energy density was boosted to 30.4 $Whkg^{-1}$ in power density of 1.27 $kWkg^{-1}$ 5 Ag^{-1}. Therefore, porous carbon nanospheres from novel STF biomass are ideal candidates as electrode materials for high-performance electrochemical energy storage devices.

INTRODUCTION

In the last decade, electrochemical energy storage devices have been developed rapidly and applied in the industrial sector, such as batteries, fuel cells, and supercapacitors.[1–4] Batteries and fuel cells are considered not to meet the need for effective, efficient, and sustainable green energy storage due to their limited lifetime and toxic-corrosive residues, although lithium-ion batteries display different performances. Due to their good performance in terms of high power density and reversibility fast charge–discharge, and long cycle life,[5–7] supercapacitors have attracted much attention as high-power energy storage devices.[8,9] Supercapacitors are promising green energy storage that can be applied in various devices such as electric vehicles, smart power grids, dynamic braking, and important components of laser systems.[10] However, the relatively low energy density of supercapacitors hinders their practical application in energy storage.[11,12] This makes it necessary to develop strategies for increasing the energy density capability without reducing its power and life cycle.[13]

Electrode-based material is the main key to improving the performance of supercapacitors, especially in increasing their energy density. Several basic materials that have been investigated to be

(Received January 6, 2023; accepted March 16, 2023)

Published online: 06 April 2023

used as supercapacitor electrode materials include metal oxides, polymers, graphene,[14,15] and carbon nanotubes.[16] However, these materials have limitations because of the high production costs, complicated synthesis processes,[17] and harmful effects on the environment.[18] Previous studies also reported that carbon materials have a high potential as high-quality electrode materials due to their low cost, sustainability, good electrical conductivity, high porosity, promising chemical stability, and large specific surface area.[19–23] In addition, materials derived from biomass are relatively easy to obtain and abundantly available, and a sustainable-pollution-free approach makes them very environmentally benign. Furthermore, activated carbon has wider applications in air purification, water treatment, energy storage, and CO_2 capture.[24] This gains activated carbon gain much attention, especially as raw electrode materials, because they can significantly improve the electrochemical performance of supercapacitors.[25] The increase in surface area does not always support high-performance capacitive supercapacitors. This is due to the assumption of a micropore structure that contributes to the high surface area that is not fully accessible in the formation of the electrical double layer. The high surface area also allows the degradation of the electrical conductivity of the electrode material, which significantly affects the reduction of the high power of electrochemical energy storage devices.

Recent studies have suggested that the electrochemical performance enhancement is not only dependent on the high surface area, but also determined by the diverse pore size distribution (micro, meso, and macroporous), 2D nano morphology (nanosphere, nanosheet, and nanofiber), and heteroatom dopant (N, O, P, S, B).[26] Therefore, optimizing the modification of the pore architecture is the best way to improve the supercapacitor performance. Modification of electrodes with interconnected hierarchical pore structures in the ranges of micro, meso, and macro is an option because it can increase the energy density of supercapacitors.[27–29] Micropores increase the specific surface area, mesopores reduce ion transport resistance, while macropores are similar to ion buffer reservoirs, which can shorten the ion diffusion distance.[30] Moreover, hierarchical pore properties can be obtained in porous carbon based on biomass waste to support sustainable and environmentally benign energy storage technologies. A porous carbon with a hierarchical pore structure has been obtained by Zheng et al.[31] from kapok flower biomass waste precursor, which exhibits outstanding electrochemical performance with a specific capacitance of 286.8 Fg^{-1}. The same result was also expressed by Xi et al.[32] who have converted cornstalk pith into 3D hierarchical porous carbon. It was discovered that the materials have increased the energy density of the supercapacitor by 13.4 Wh kg^{-1} at a significant rate capability. This hierarchical pore architecture was also confirmed in activated carbon from the precursors of alfalfa flower,[33] waste tea,[34] and jujube fruit.[35] However, the abundant 3D hierarchical pore behavior covering all surfaces of the electrode material can reduce their electrical conductivity, which limits the practical application of energy storage devices.

The 2D nano morphology with a uniform structure significantly affects the increase in the electrical conductivity of the electrode material. Nanospheres as one of the 2D nanoscales have gained significant attention as supercapacitor electrodes due to their distinctive shape with unique advantages such as uniform geometry, high density, and good conductivity.[36] According to Zheng et al. (2021), nanosphere structures have shown their tremendous potential in enhancing the performance of supercapacitors.[37] They have demonstrated a nanosphere morphology with an outstanding cyclical performance of $\sim$ 96.5%. Hollow microporous carbon nanospheres were obtained by simply treatment of KOH-activated pyrolyzing with a retention capacitance of 86.7%.[38] Nickel–cobalt-based nanospheres obtained through metal–organic framework (MOF) techniques have also confirmed their high performance with an outstanding energy density of 55.4 Wh kg^{-1} at a cyclical performance of 98.8%.[39] However, the original materials and methods applied have drawbacks. This is because the materials used are not environmentally friendly; they are corrosive, toxic, and expensive, followed by complicated, tedious, and time-consuming procedures, limiting their production on a large scale.[37,40] Meanwhile, biomass-based carbon nanospheres offer good density, evenly distributed pores, and defined particle size through synthesis techniques that are more environmentally friendly, sustainable, and free of toxic/corrosive residues. This is to provide a good ion transport pathway on the surface of carbon electrodes without reducing their high electrical conductivity.[37] Shallot peel biomass has recently been converted as carbon nanosphere through multiple activations without applying complicated techniques such as MOFs, templates, or strobe. The carbon nanofibers obtained have oxygen as a self-doping heteroatom function, which can increase the supercapacitor energy density by 16.7 Wh kg^{-1}.[41] The carbon nanosphere obtained from the biomass precursor corn straw has also been applied to the anode material for lithium-ion batteries.[42] This reveals the great potential of biomass as a carbon nanosphere source for electrochemical energy storage applications. This potential is still difficult to obtain and poses a serious challenge. This showed that there is a need to develop carbon nanofiber-based electrode materials from biomass materials.

Solanum torvum is a shrub that thrives in Indonesia, especially in Java and Sumatra islands. This plant is commonly known as Turkish berry and is widely distributed in tropical areas ranging from

Indonesia, Malaysia, Philippines, Pakistan, India, tropical America, Africa, and the West Indies.[43,44] *Solanum torvum* fruits (STF) have a uniform spherical shape with a diameter ranging from 2 to 3 cm, which is rich in lignin and cellulose, enabling them to be a porous carbon source. The unique geometric shape also indicates their potential to present the nanosphere structure. Moreover, this is the first and most recent report on the potential of STF fruit as a carbon source with a nanosphere structure for supercapacitor applications.

In this study, activated carbon nanospheres with unique 3D "cow tripe-like" hierarchical pores were obtained from novel biomass of STF through an easy, green, environmentally benign, sustainable, and toxic-corrosive-free technique for electrochemical energy storage applications. STF was converted to porous carbon through a combination of pre-carbonization, chemical impregnation of $ZnCl_2$, carbonization, and physical activation. The pore structure and surface morphology were controlled using activating agent concentrations at 0.3 M, 0.5 M, and 0.7 M, respectively. The optimized porous carbon displayed enriched nanosphere morphology, followed by an abundant hierarchical "cow tripe-like" pore structure with a high specific surface area of 1176.29 $m^2\ g^{-1}$. They also indicated the self-doping of functional oxygen, thereby increasing the capacitive behavior of the electrode material. The best electrochemical properties of supercapacitor cells were obtained with a specific capacitance of 154 $F\ g^{-1}$ in 1 M H_2SO_4 electrolyte in a two-electrode system. Furthermore, its energy density was increased by 30.4 Wh kg^{-1} at a current density of 1 $A\ g^{-1}$. These results indicated the great potential of STF as a source of hierarchical porous carbon nanospheres to improve the electrochemical properties of supercapacitor energy storage devices.

MATERIALS AND METHODS

Materials

Solanum torvum fruit (STF) was harvested from a plantation in Pekanbaru, Indonesia. Meanwhile, zinc chloride ($ZnCl_2$) for chemical activation was obtained from Emsure KgaA. Sulfuric acid (H_2SO_4) as an electrolyte was purchased from Panreac Quimica S.A.U. Distilled water was used to neutralize the sample and a 0.1 mm-thick duck eggshell membrane as a separator.

Preparation of STF Materials

STF was crushed using a chopper until it became a slurry. The sample was dried using a drying oven at 110 °C and pre-carbonized through a vacuum oven at 250 °C for 2 h 30 min. Furthermore, the samples were produced by grinding using a mortar and milling. The sample powder from the milling was sieved using a 60 μm sieve to obtain a uniform-size STF powder precursor.

Preparation of Activated Carbon

Activated carbon from STF was prepared by chemical activation using zinc chloride ($ZnCl_2$) and one-step pyrolysis via carbonization and physical activation. The 30 g of precursor powder was mixed with $ZnCl_2$ solution at different concentrations such as 0.3 M, 0.5 M, and 0.7 M. The mixture was stirred using a hotplate at 80 °C with a rotation rate of 300 rpm. To facilitate data analysis, each sample was labeled with a code STF-3, STF-5, and STF-7 corresponding to the concentration of the activating agent applied. Subsequently, the chemically activated carbon sample was dried in a drying oven and printed using a hydraulic press with a pressure of 8 metric tons to obtain coins/pellets form. The pellets formed were ± 2 cm in diameter with a thickness of ± 0.2 cm. Subsequently, they were carbonized using N_2 gas in a furnace from a temperature of 30°C–600°C, followed by physical activation characterized by the conversion of N_2 gas to CO_2 at 600°C, which started from a temperature of 600°C–800°C for 2 h 30 min. The coin-shaped carbon obtained from the pyrolysis results was cooled to room temperature and washed using distilled water. This washing was repeated for 5–6 days until the pH was neutral (7), and the washed carbon was dried for 24 h. In detail, preparation of hierarchical porous carbon nanospheres based on *S. torvum* fruit is shown in Fig. 1.

Material Characterization

The mass, diameter, and thickness were measured to determine the density of carbon pellets calculated through standard equations. The surface morphology of the samples was investigated by scanning electron microscopy (SEM) using the Zeiss Evo 10 instrument. The phase and degree of crystallinity of the samples were examined using x-ray diffraction (XRD) techniques on X-Pert Powder Panalytical instruments with Cu K-α light sources in the range scattering angle 2θ at 10°–60°. The porosity properties of STFs such as surface area and pore structure were reviewed through the N_2 gas absorption technique at 77 K using Quantachrome Touchwin V1.22. The specific surface area was obtained from the Brunauer–Emmett–Teller (BET) method. Furthermore, the T-Plot method was used to calculate the pore volume and surface area of the micropores as well as for the pore size distribution obtained from the calculation of the Barrett-Joyner-Halenda (BJH) equation.

Supercapacitor Cell Performance Evaluation

The supercapacitor device consists of two electrodes made of STF, a duck eggshell membrane as a separator, and 1 M H_2SO_4 as an electrolyte. The performance of supercapacitor cells was evaluated by cyclic voltammetry (CV) and galvanostatic charge discharge (GCD) methods on a two-electrode

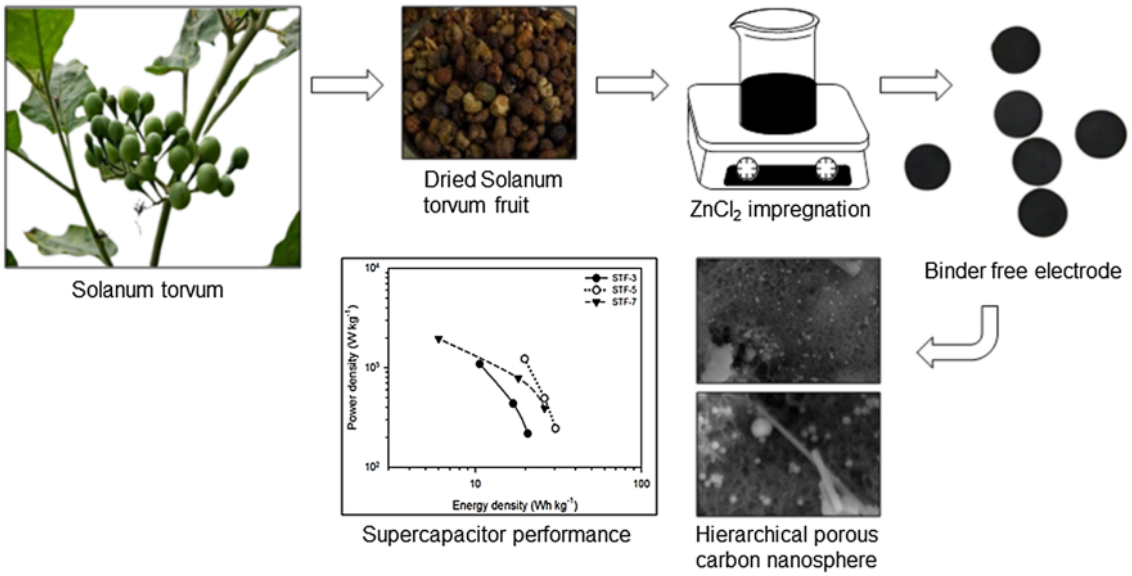

Fig. 1. Preparation of hierarchical porous carbon nanosphere based on *Solanum torvum* fruit.

figuration system. CV testing was carried out at scan rates of 1 mV s^{-1}, 2 mV s^{-1}, and 5 mV s^{-1} using the CV UR Rad-ER 5841 physics tool. Subsequently, GCD testing was reviewed through the CD UR Rad-ER 2018 instrument at a current density of 1 A at a scanning rate of 1 mV s^{-1}. The electrochemical properties such as specific capacitance (Csp, F g^{-1}), energy density (E, Wh kg^{-1}), power density (P, W kg^{-1}), and resistance (R, Ω) obtained were calculated using the standard formula discussed in the previous study.

RESULTS AND DISCUSSIONS

Activated carbon from STF was evaluated for density changes as shown in Fig. 2. Evaluation of density changes is an initial review to analyze the physical properties of activated carbon in form of solid coins/monolith without adhesive. From the initial treatment to powder prepared stage, STF exhibit carbon yield of 43%. Furthermore, the carbon powder is designed in the form of solid coins/monolith without adhesive and is followed by an integrated pyrolysis stage. Before a step of pyrolysis through carbonization and physical activation, the density of STF ranged from 0.8912 g cm^{-3}, 0.8863 g cm^{-3}, to 0.9204 g cm^{-3}. After pyrolysis, the density of all samples based on concentration variations decreased with values of 0.5211 g cm^{-3}, 0.3608 g cm^{-3}, and 0.5357 g cm^{-3} in STF-3, STF-5, and STF-7 samples, respectively. In addition, activated carbons of STF-3, STF-5, and STF-7 obtained from the integrated pyrolysis stage exhibit carbon yields of 83.33%, 84.61%, and 80.59%, respectively. This is due to the influence of the carbonization process and physical activation

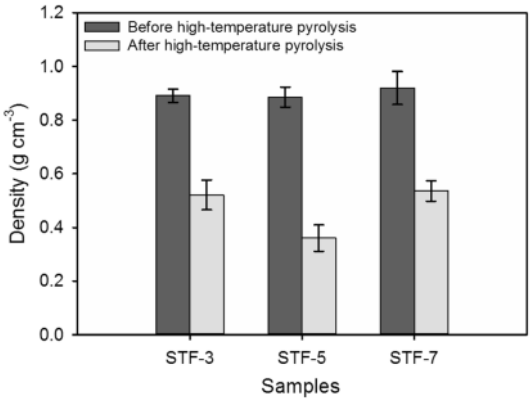

Fig. 2. Density of STF electrodes.

that causes the evaporation of volatile non-carbon compounds and reduces the dimensions of the monolith, including mass, volume, and density.[45] The carbonization process in an N_2 gas environment from 30 °C to 600 °C decomposes water, minerals, and all complex compounds including hemicellulose, cellulose, and lignin to reduce the volatile content, which yields a high carbon content.[46] The by-product of the carbonization process in form of tar inhibits the carbon pores that are formed; therefore, a physical activation process is needed in a CO_2 gas environment.[47] The physical activation process from 600 °C to 800 °C aims to maximize tar reduction to form a better pore structure.[48] The combination of these two processes can increase porosity, causing a decrease in sample density. The impregnation of the

selected chemical activating agent significantly affects the dimensions of the coin solid carbon design. Increasing the concentration of $ZnCl_2$ from 0.3 to 0.5 M allows continuous etching of the carbon chain, which reduces the mass and volume of the sample precursor. This simultaneously presents abundant empty spaces improvising their porosity. Therefore, STF-5 showed the highest density reduction of 58.47%. However, an increase in the concentration of the activating agent to 0.7 M showed a decreased density reduction of about 41.71%. This is due to the excessive carbon chain etching that erodes the foundation of the precursor pore framework and cannot maintain the hierarchical pore structure, leading to the collapse of the various pore surfaces and covering the underlying pores.[49]

The novel biomass STF with a uniform spherical shape was converted to a porous activated carbon with a unique 2D nanosphere structure through the green, environmentally benign, and non-corrosive-toxic method. It was discovered that chemical activation using $ZnCl_2$ in 0.5 M solutions followed by high-temperature pyrolysis with N_2 and CO_2 gas eroded lignocellulosic compounds to present a unique 2D nanospherical shape. The morphology of the porous activated carbon nanospheres from STF was confirmed using scanning electron microscopy as shown in Fig. 3. The result showed that the STF-5-based carbon shows a highly interconnected 3D hierarchical pore morphological structure and uniform solid nanospheres, illustrating the unique "cow tripe-like" shape. Hierarchical pores have been confirmed in the mesoporous and macropores ranges. Furthermore, Fig. 3a shows SEM images at 5000 magnification, revealing highly abundant nanospherical morphological structures on all precursor surfaces. The 2D nanospheres were found in all chunks, aggregates, and inner carbon blocks. In a larger area, the SEM images confirmed the rich hierarchical pores that are interconnected with each other resembling a unique "cow tripe-like" shape as shown in Fig. 3b. Furthermore, the nanospheres were evenly distributed in the hierarchical pores, which allow the porous carbon material to have high porosity properties and maintain good electrical conductivity for the supercapacitor electrodes. In this area, 2D nanospheres were found with diameters ranging from 162 to 519 nm, while the hierarchical pore morphology at the nanoscale was between 108 and 471 nm. In the high-temperature carbonization and pyrolysis processes, chemical activators hydrate and degrade complex lignocellulosic compounds, including lignins, that make important contributions in showing tubular structures and are speculated to present nanospheres on carbon-based biomass. The early reaction of $ZnCl_2$ impregnation also allows high exploitation of the precursor potential to completely etch the carbon chain, leading to a unique hierarchical "cow tripe-like" pore structure. The shallow 3D interconnected pore shape allows the biomass carbon-based electrode materials to optimize the insertion/de-insertion of ionic charges in all directions to form the optimum electrical double layer without compromising their high power density. At 20,000 magnification, the nanospheres and the hierarchical pores

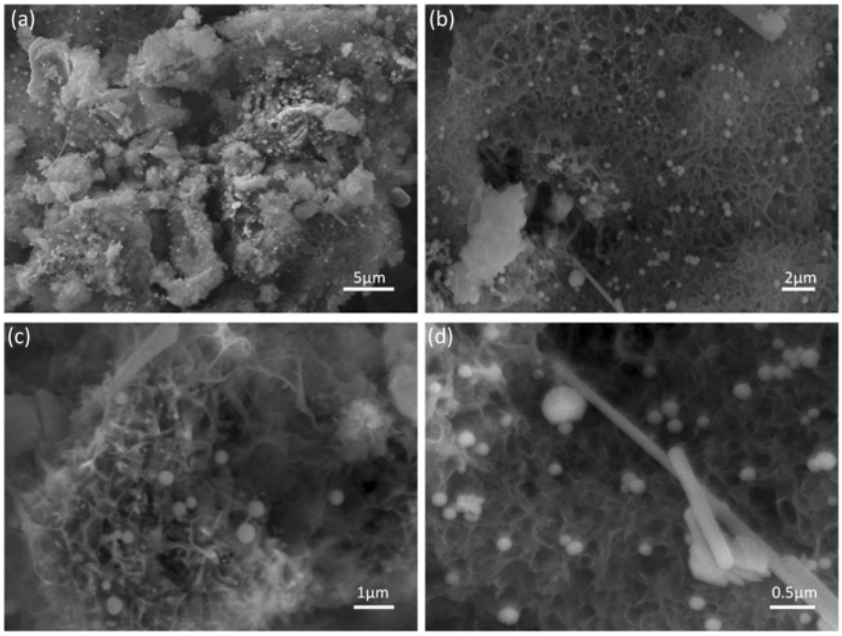

Fig. 3. (a-d) SEM image of hierarchical porous carbon nanosphere-derived *Solanum torvum* fruit (STF).

of "cow tripe-like" and rod-like structure are visible, as shown in Fig. 3c, with nanoseries size ranging from 270 to 969 nm, 184 to 467 nm, and 318 to 582 nm, respectively. Furthermore, the material has interconnected pores to form a bovine tripe pore structure, and an abundance of nanospheres contributes to enhancing the high porosity behavior and excellent electronic conductivity of the electrode material. This significantly increases the effectiveness of the electrode surface area in charge storage, and the interconnected pores can form a better electrode–electrolyte interface.[50] The existence of the structure can support high-performance electrode materials as a high-quality, environmentally benign, and pollution-free supercapacitor energy storage device.[51] A rod-like structure/fiber was also confirmed in Fig. 3d because the cellulose is being leached at high temperatures, which reduces its size.[49] The nanospheres at this magnification range in size from 205 to 423 nm, while the hierarchical pore sizes are from 65 to 561 nm. A deeper analysis is poured into the analysis of N_2 gas absorption and electrochemical performance through CV and GCD.

The x-ray diffraction pattern of porous carbon based on novel STF biomass in different concentrations of activating agents is illustrated in Fig. 4. The x-ray diffraction pattern is the output generated for STF-3, STF-5, and STF-7 samples with an angle of 2θ in the range of 10° to 60°. All samples showed the presence of two broad peaks, each of which is located in a different hkl plane of 002 and 100 scattering planes. This broad peak occurred because of low crystallinity; therefore, the activated carbon electrode is amorphous.[52] The wide peaks in the scattering planes 002 and 100 with scattering angles ranging between 21°–25° and 42°–45° indicate that the porous carbon STF has good electrical conductivity.[53] This characteristic pattern of initiating abundant micropore structures was confirmed at the gently shifting peaks of the 002 scattering plane. The 002 scattering field shifts from 25 to 21 frequently with increasing concentrations of the

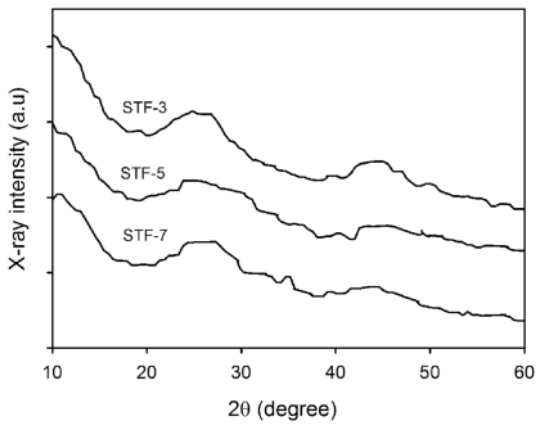

Fig. 4. XRD pattern of STF samples.

$ZnCl_2$ activating agent, which indicates the development of their narrower pores due to the reaction of carbon with an intense activating agent as shown in Table II. The behavior of the rich micropores is required to provide suitable ionic charge sites for accessibility at the electrode/electrolyte interface. This characteristic XRD pattern is similar to that of several previous investigations, which also showed similar x-ray diffraction characteristics such as activated carbon from tea waste biomass precursors,[54] garden waste,[17] neem leaves,[55] bark waste potatoes,[56] and argan shells[57].Table I shows the parameter data of the carbon lattice of *S. torvum* fruit, which experienced a shift in the scattering angle causing changes in the value of layer height (L_c) and layer width (L_a) and showing the distance between the planes (d_{002}) and (d_{100}). According to the Bragg $2d\sin\theta = n\lambda$ equation, the average distance between layers d_{002} and d_{100} ranged from 0.348 nm to 0.419 nm and 0.200 nm to 0.204 nm, respectively. The d_{002} value obtained was higher than the normal graphite d_{002}; this indicated that STF carbon has weak graphite properties with better amorphous properties, which initiate the formation of high porosity. The value of the layer height (L_c) is related to the prediction of the specific surface area of the carbon material according to the empirical equation $SSA = 2/\rho_{xrd}L_c$. The SSA value obtained for the STF-3 sample is 1230 $m^2\ g^{-1}$, while for the STF-5 and STF-7, the values are 2244 $m^2\ g^{-1}$ and 1830 $m^2\ g^{-1}$, respectively. This indicated that a small L_c value can support the formation of an active site suitable for ion diffusion at the electrolyte/electrode interface.[58]

The porosity properties of 2D carbon nanospheres based on STF were evaluated using Brunauer Emmett Teller (BET), t-Plot, and Barrett Joyner Halenda (BJH) methods to obtain specific and microporous surface area, as well as pore size distribution. Figure 5a and b illustrates the nitrogen adsorption–desorption profiles and the pore size distribution of STF-3, STF-5, and STF-7. Moreover, the characterization results for STF showed a type I and IV collaboration isotherm curve with an H4-type hysteresis loop.[59] At relatively low-pressure, P/P0 < 0.1 indicates an increase in the absorption volume due to the presence of abundant micropores, which continue until a higher pressure of 0.4 < P/P0 < 0.91. This is followed by an H4 hysteresis loop, indicating the presence of a well-developed mesopore. At relatively high pressures, a slightly increased slope confirms the presence of macropores.[60,61] This indicated that a hero pore structure with high porosity was obtained by chemical activation of $ZnCl_2$ in the STF biomass, as shown in Fig. 3. Furthermore, the difference in concentration of $ZnCl_2$ in STF-activated carbon had a significant effect on the specific surface area and pore volume. The addition of an activator concentration of 0.3 M to 0.5 M increased the surface area and pore volume as presented in Table II. In STF-3, the surface area

Table I. Interlayer spacing and lattice parameter for carbon of *Solanum torvum* fruit (STF)

Sample	$2\theta_{002}$ (°)	$2\theta_{001}$ (°)	d_{002} (Å)	d_{100} (Å)	L_c (Å)	L_a (Å)
STF-3	25.512	45.172	3.488	2.005	7.455	27.909
STF-5	23.272	44.304	3.819	2.042	5.691	7.822
STF-7	21.145	44.350	4.198	2.040	6.030	12.834

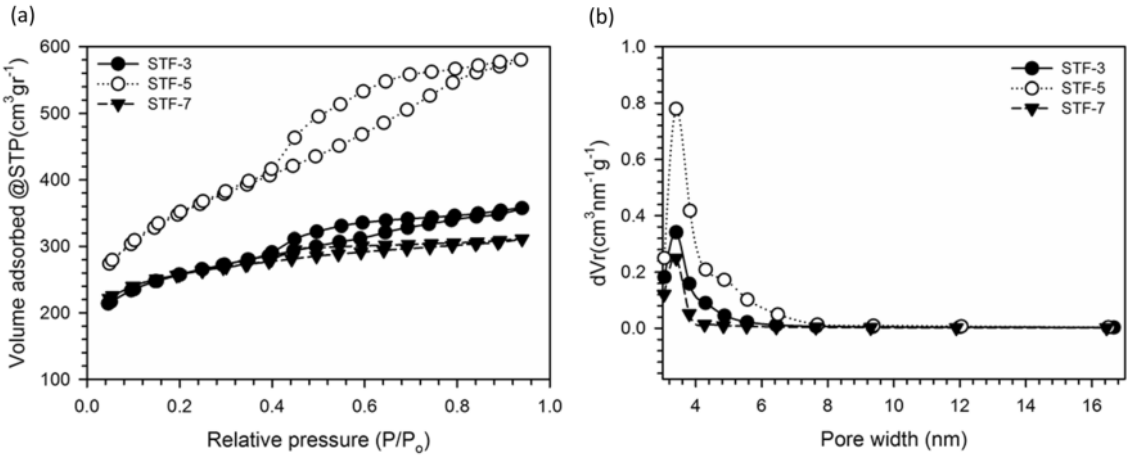

Fig. 5. (a) Nitrogen adsorption–desorption profiles of STF samples and (b) pore size distribution of STF samples.

Table II. Porosity properties of STF samples

Sampel	S_{BET} ($m^2\ g^{-1}$)	S_{micro} ($m^2\ g^{-1}$)	S_{meso} ($m^2\ g^{-1}$)	v_{tot} ($cm^3\ g^{-1}$)	D_{aver} ($cm^3\ g^{-1}$)
STF-3	839.959	535.526	304.433	0.554049	1.31923
STF-5	1176.29	544.006	632.289	0.899726	1.52976
STF-7	821.09	628.164	192.926	0.482467	1.17519

value was 839.959 $m^2\ g^{-1}$ with a pore volume of 0.554049 $cm^3\ g^{-1}$ and increased in STF-5 with a surface area value of 1176.29 $m^2\ g^{-1}$ and the pore volume of 0.899726 $cm^3\ g^{-1}$. This increase occurred because of the $ZnCl_2$ activator, which acts as a reducing agent and breaks the lateral bonds in the cellulose molecule to produce activated carbon with a high surface area. STF-5 also shows significant mesoporous productivity, as presented in Table II. This nearly balanced combination of micro- and mesopores is very advantageous for optimizing the high performance of electrode materials in producing high energy density and power in supercapacitor electrochemical energy storage devices. The pore size distribution in the carbon nanosphere is illustrated in Fig. 5b. STF-5 shows an abundant mesopore size distribution compared to STF-3 and STF-7. This reinforces the presence of hierarchical pores in STF-5, supporting the high performance of their electrodes. However, at STF-7, the specific surface area was reduced to 821.09 $m^2\ g^{-1}$ and the total pore volume was 0.482467 $cm^3\ g^{-1}$. This decrease occurred because of damage to the hierarchical pore framework because of excessive etching of carbon chains by $ZnCl_2$ at a concentration of 0.7 M for the pores that had been formed to collapse and cover the well-formed pores underneath.[62] On the plus side, the more carbon chain etching on ST-7 allowed the precursor to having higher micropores than STF-3 and STF-5, as presented in Table II. The predominant micropores can support electrochemical performance with high surface area contributed and energy densities through maximum ion absorption.[63] The availability of a large number of mesopores also provides benefits for rapid ion transfer, which favors enhanced electrochemical performance.[30] This showed that the combination of pores can improve the performance of high storage applications, especially energy and power density.[64] Therefore, it is concluded that the high surface

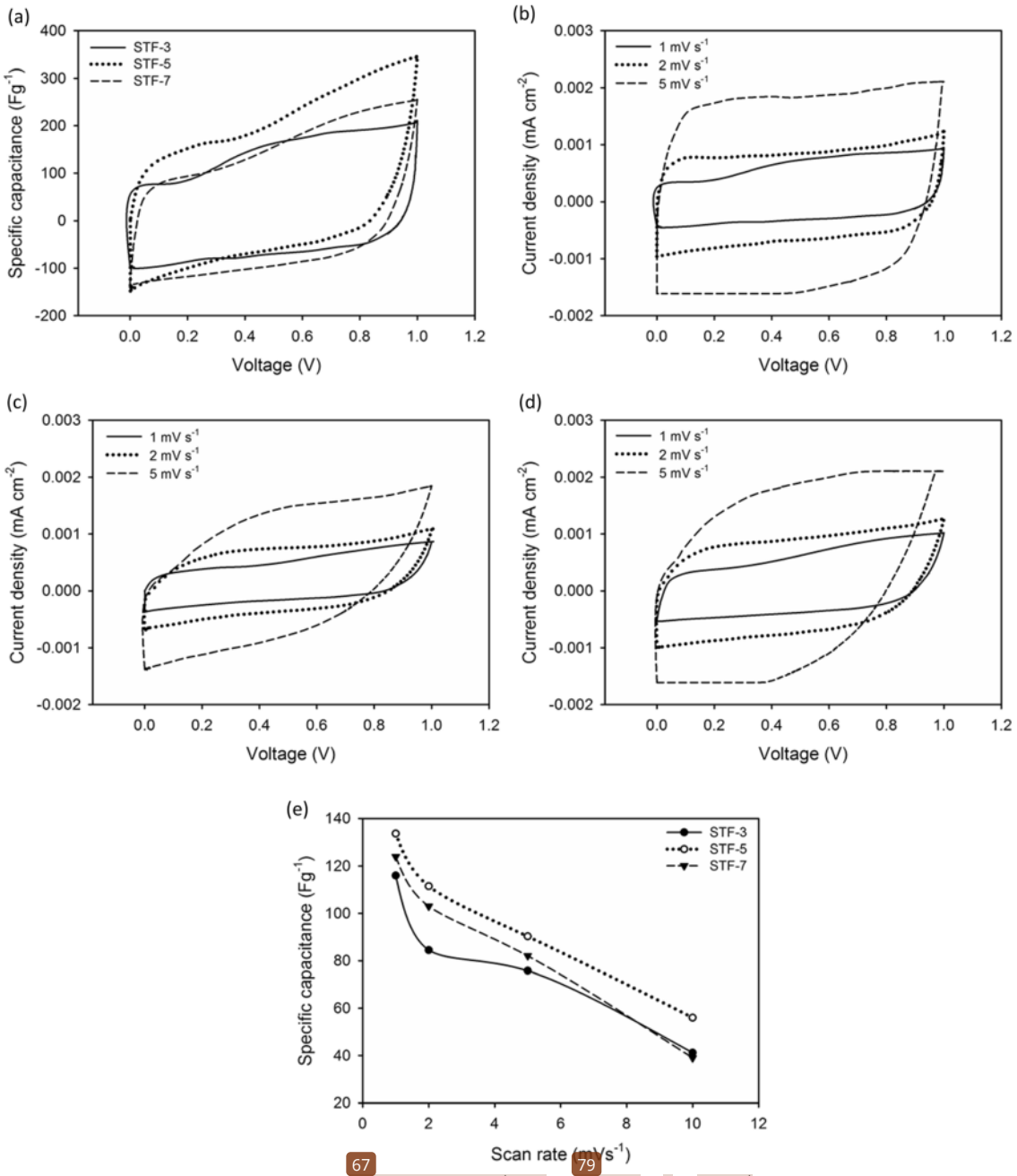

Fig. 6. CV profile of STF samples in H_2SO_4 (a) at scan rate of 1 mV s^{-1}, (b-d) at scan rate of 1- 5 mV s^{-1}, (e) specific capacitance vs. scan rate in 1 M H_2SO_4.

area with elevated pore volume and hierarchical porosity can facilitate easy ion transport and charge storage for prepared STF-5 to have a high potential for electrode materials in supercapacitor applications.[65]

The electrochemical performance of the STF-based carbon nanosphere for supercapacitor cell was evaluated using cyclic voltammetry (CV) and galvanostatic charge discharge (GCD) methods in a two-electrode configuration immersed in 1 M H_2SO_4

electrolyte. Figure 6a shows the CV curves of the STF-3, STF-5, and STF-7 electrodes at a scan rate of 1 mV s^{-1} with potential intervals from 0.0 to 1.0 V. The CV curve shows a distorted rectangular shape characterizing the ideal electrical double-layer capacitance behavior for biomass-based activated carbon nanosphere electrodes.[66,67] The STF electrode also shows a curve with a fast specific capacitance response at low voltages < 0.08 V. This is due to the fast diffusion of ions in the electrolyte towards the electrode surface, where the rich micropores are filled with ions to form a charge layer on the electrode/electrolyte interface. At voltages > 0.1 V, the capacitance response begins to subside, because the ion charge has filled the larger pores until the maximum voltage reaches 1.0 V.[68] The STF-3 displays a rectangular shape followed by a potential hump of 0.2–0.8 V confirming the presence of pseudocapacitance effects derived from faradaic redox reactions. Functional oxygen contributes as a self-doping heteroatom, which enables a pseudocapacitance effect on the STF-3 electrode. However, STF-3 shows the smallest rectangular shape indicating low material properties to improve the electrochemical properties of the supercapacitor electrodes. The STF-5 electrode shows a wider rectangular shape compared to STF-3 and STF-7, confirming the high double-layer capacitance.[52] The addition of the activating agent concentration from 0.3 M to 0.5 M significantly increases the specific surface area. This allows the provision of multiple active sites in the STF-5 electrode, thereby forming an abundant electrochemical double layer. The high mesoporosity contributes to the smooth flow of ionic charges at the electrode/electrolyte interface, thereby increasing the high performance of the STF-5 electrode. The addition of higher concentrations can reduce the wettability of the samples through the evaporation of oxygen in form of CO_2 and H_2O, as confirmed in the CV profile of STF-5, which reduced their pseudocapacitance effect. A further increase in concentration up to 0.7 M shows a smaller rectangular shape than STF-5. This is because the STF-7 experienced a decrease in the specific surface area as discussed in the N_2 gas absorption analysis, thereby reducing their high electrochemical properties. Therefore, it can be concluded that STF-5 has the highest capacitive behavior, followed by STF-7 and STF-3. The high performance of the STF electrodes was also observed at high sintering rates from 1 mV s^{-1} to 5 mV s^{-1}, as shown in Fig. 6b, c and d. At a high scan rate of 5 mV s^{-1}, the CV profiles of STF-3, STF-5, and STF-7 retaining a rectangular shape exhibit better EDLC properties.[67] The pseudocapacitance effect of functional oxygen as self-doping oxygen was degraded, revealing weak faradaic redox reactions in STF carbon nanosphere-based electrode materials. The capacitive properties of STF electrodes at different scanning rates are illustrated in Fig. 6e. It was discovered that the specific capacitance decreases as the scanning rate increases because of their unbalanced pore distribution, which impedes electrolyte ion transport at high scanning rates.[69] This is called the diffusion limit, where it is difficult for electrolyte ions to diffuse into the pores of the electrode. There is an ineffective interaction between the electrode material and the electrolyte for the specific capacitance to decrease at high scanning rates.[70] The STF-5 electrodes show good cyclical performance by maintaining their specific capacitance of about 56% at a scan rate of 5 mV s^{-1}.

The electrochemical properties of STF carbon nanosphere electrodes were evaluated using galvanostatic charge–discharge (GCD), especially for specific capacitance, power density, and energy density. The GCD profile for an STF-based carbon nanosphere electrode immersed in 1 M H_2SO_4 electrolyte at a current of 1 A g^{-1} is shown in Fig. 7a. The GCD profile revealed an imperfect isosceles triangle shape that indicated the characteristic electrical double-layer properties.[71] This is in line with the CV profile shown in Fig. 6 where the type of distorted isosceles triangle showed the reversibility of different ion charge–discharge times for each STF due to ion degradation caused by self-heteroatom, which shows a pseudocapacitance effect. The functional oxygen in form of OH/COOH on the electrode surface allows the addition of wettability properties to initiate faradaic redox reactions in the charging process. It is characterized by a convex curvature of the GCD profile. The low IR drop confirmed the STF electrode resistance of 0.155 Ω, 0.069 Ω, and 0.027 Ω for the STF-3, STF-5, and STF-7 electrodes. Lower resistance indicates higher conductivity along with the addition of $ZnCl_2$, which can increase the conductivity of the electrode.

The length of charging and discharging time indicates the high capacitive nature of the STF electrode.[72] In this study, STF-3 has a shorter charge and discharge time, showing that the electrode has a smaller specific capacitance of 118 F g^{-1}. The specific capacitance increased at STF-5, which was characterized by a longer charge and discharge time with a specific capacitance of 154 Fg^{-1}. This increase was influenced by the $ZnCl_2$ activator, which significantly increased the specific surface area from 839,959 m^2 g^{-1} to 1176.29 m^2 g^{-1}. The combination of 2D nanospheres and the unique 3D interconnected shallow “cow tripe” pore shape also allows the biomass carbon-based electrode material to have unique advantages such as uniform geometry, good density, well-distributed porosity, and well-defined particle sizes to optimize the insertion/de-insertion of ionic charges in all directions from the optimum electrical double layer without compromising their high power density.[73] The addition of the activating agent at 0.7 M led to a reduction in the specific surface area and a widening of the pore size, thereby reducing the specific capacitance by 14.93% to 131 F g^{-1}. The coulombic efficiency of the

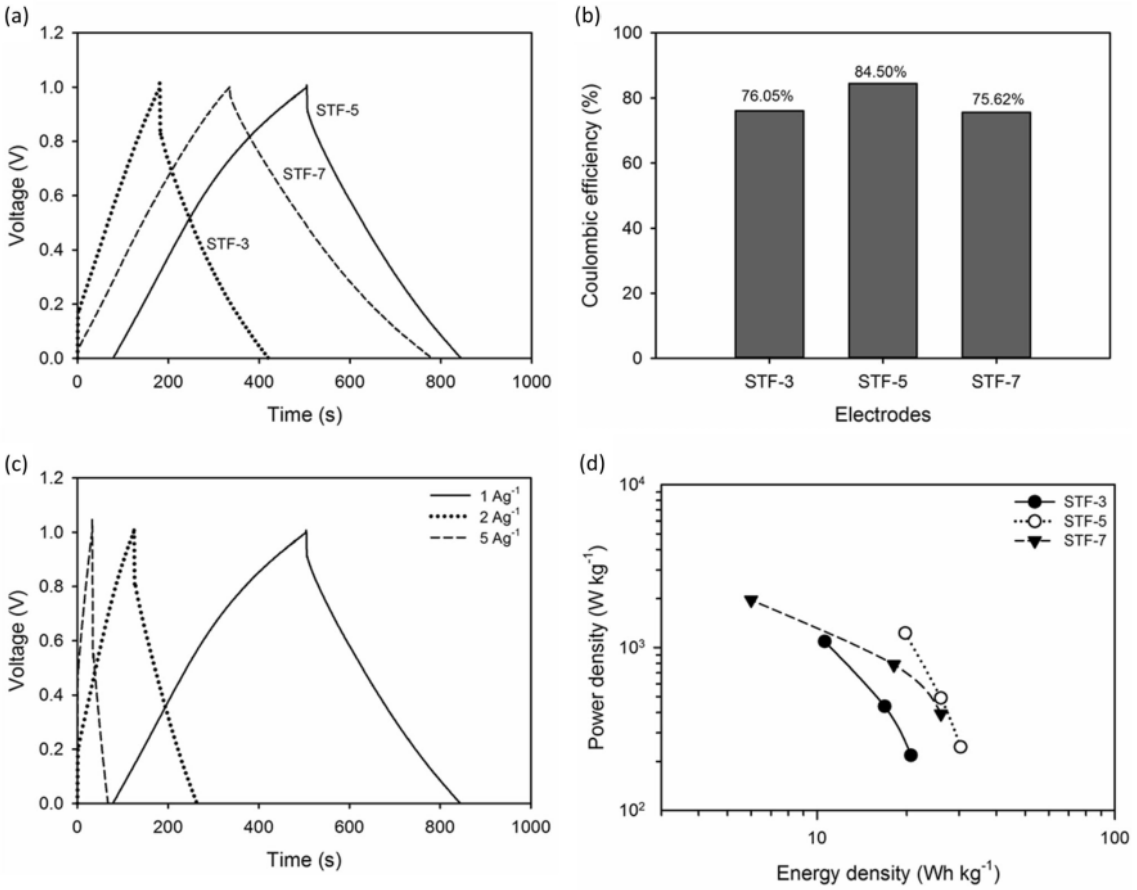

Fig. 7. (a) GCD profile of STF samples in H_2SO_4 at a current of 1 A g^{-1}, (b) Coulombic efficiency of the STF electrodes, (c) GCD profile of STF-5 at a current of 1–5 A g^{-1}, and (d) Ragone plot of STF samples.

STF electrode was also implemented through the ratio between charge and discharge time on the GCD curve, as shown in Fig. 7b. This shows that the coulombic efficiency obtained for STF-3, STF-5, and STF-7 were 76.05%, 84.50%, and 75.62%, respectively. This proves that the STF-5 electrode has the best electrochemical performance compared to the STF-based carbon nanosphere source. The high electrochemical confirmation of the STF-5 electrode was examined by different current densities from 1 A g^{-1} to 5 A g^{-1}, as shown in Fig. 7c. Based on Fig. 7c, the GCD profile still maintains the distorted isosceles triangle shape, revealing good electrical double-layer properties. The STF-5 electrode shows that the charge–discharge time confirms the charge storage phenomenon, where the high current density hinders the electrolyte ions from having sufficient time to diffuse to complete the faradic reaction at the electrode surface.[74] This causes the electrochemical performance to reduce for the capacitance to decrease as the current density increases. The STF-5 electrodes maintained their high specific capacitance of 101 F g^{-1} at 5 A g^{-1} in the two-electrode configuration system.

The energy and power densities of the STF carbon nanosphere electrode were fully evaluated as shown in the Ragone plot of Fig. 7d. STF-5 electrode showed the highest energy density of 30.43 Wh kg^{-1} with a maximum power density of 1.27 kW kg^{-1} at a current density of 5 A g^{-1}. Meanwhile, the STF-3 and STF-7 electrodes have lower energy densities of 26 Wh kg^{-1} and 19 Wh kg^{-1} at power densities of 1.10 k and 800 W kg^{-1}, respectively. These results were compared with other biomass-based carbon sources, as shown in Table III.

CONCLUSION

A simple, green, sustainable, and corrosion/toxin-free synthesis route was demonstrated to obtain carbon nanosphere with a unique hierarchical pore "cow tripe-like" structure from the novel biomass of

Table III. Comparison of the electrochemical performance of carbon biomass-based for supercapacitor electrodes

Sources	Morphological structure	S_{BET} (m^2g^{-1})	Electrode type	Electrolyte	E_{sp} (Wh kg^{-1})	P_{sp} (W kg^{-1})	References
Camellia japonica flowers	Interconnected spherical	–	3-electrode	1 M KOH	34.54	1600	75
Tea saponin	Sheet	1550.3	2-electrode	1 M TEABF4	27.01	1500	53
Chitin	Hierarchical porous	1158.69	3-electrode	6 M KOH	22.07	980	76
Seaweed powder	3D honeycomb	1206.97	3-electrode	6 M KOH	3.125	5000	77
Camphor leaves	Hierarchical porous	2794	3-electrode	6 M KOH	32.9	9461	78
Lemon peel	Sheet	–	3-electrode	1 M H_2SO_4	11.84	361.8	79
Foxtail grass seeds	Hierarchical porous	1428	3-electrode	6 M KOH	18.2	–	80
Wheat husk	Hollow tunnels	1200	3-electrode	6 M KOH	–	–	81
Onion peel	Hierarchical porous	–	3-electrode	1 M H_2SO_4	13.61	200.8	82
Lessonia trabeculata macroalgae	Highly coupled flake	769	2-electrode	1 M KOH	2.82	491	83
Solanum torvum fruit	Hierarchical porous carbon nanosphere	1176.29	2-electrode	1 M H_2SO_4	30.4	1270	This work

STF for high-performance supercapacitors. The pore structure, morphology, and electrochemical properties of activated carbon nanospheres were reviewed with the application of three different concentrations of $ZnCl_2$ activating agent. The STF-5 sample significantly confirmed the extraordinary potential of STF biomass to obtain activated carbon with a combination of rich nanosphere structure and unique "cow tripe-like" hierarchical pores. Furthermore, the impregnation of $ZnCl_2$ at high-temperature pyrolysis also increased the porosity of the high carbon nanosphere by 1176.29 m^2 g^{-1} with a very rational micro:meso distribution. The symmetrical supercapacitor assembled based on STF-3 electrodes exhibited a specific capacitance of 154 F g^{-1} and an increased energy density output of 30.4 Wh kg^{-1} at 1 A g^{-1} in aqueous electrolyte H_2SO_4. Based on this result, it can be concluded that the novel biomass optimized through the proposed strategy is highly efficient and effective to obtain activated carbon with hierarchical porous nanosphere regulation as a promising electrode material for high-performance supercapacitor applications.

ACKNOWLEDGEMENTS

The research was financially supported by second Batch Project of Word Class Research (WCR) in *Kementerian Pendidikan, Kebudayaan, Riset, dan Teknologi,* Republic of Indonesia, with the title "High energy and power densities of supercapacitor for the optimization of electrode supply process" Contract No. 1627/UN19.5.1.3/PT.01.03/2022.

CONFLICT OF INTEREST

The authors declare that they have no conflict of interest.

REFERENCES

1. X. Zhu, X. Huang, S. Anwer, N. Wang, and L. Zhang, *Langmuir* 36, 9284 (2020).
2. H. Sun, J. Zhu, D. Baumann, L. Peng, Y. Xu, I. Shakir, Y. Huang, and X. Duan, *Nat. Rev. Mater.* 4, 45 (2019).
3. J. Niu, R. Shao, M. Liu, Y. Zan, M. Dou, J. Liu, Z. Zhang, Y. Huang, and F. Wang, *Adv. Funct. Mater.* 1905095, 1 (2019).
4. P.R. Kharangarh, N.M. Ravindra, G. Singh, and S. Umapathy, *Energy Storage* 5, e390 (2022).
5. N. Yadav, P. Ritu, and S.A. Hashmi, *Sustain. Energy Fuels* 4, 1730 (2020).
6. P.R. Kharangarh, N.M. Ravindra, R. Rawal, A. Singh, and V. Gupta, *J. Alloys Compd.* 876, 159990 (2021).
7. P. Bhardwaj, S. Singh, P.R. Kharangarh, and A.N. Grace, *Diam. Relat. Mater.* 108, 107989 (2020).
8. Z. Bi, Q. Kong, Y. Cao, G. Sun, F. Su, X. Wei, X. Li, A. Ahmad, L. Xie, and C.-M. Chen, *J. Mater. Chem. A* 7, 16028 (2019).
9. P.R. Kharangarh, V. Gupta, A. Singh, P. Bhardwaj, and A. Umala, *Diam. Relat. Mater.* 107, 107913 (2020).
10. F. Guo, Y. Jiang, Z. Xu, H. Wang, and C. Gao, *Nat. Commun.* 9, 1 (2018).
11. S. Kumar, G. Saeed, L. Zhu, K. Nam, N. Hoon, and J. Hee, *Chem. Eng. J.* 403, 126352 (2021).
12. P.R. Kharangarh, N.M. Ravindra, G. Singh, and S. Umapathy, *J. Energy Storage* 55, 105388 (2022).
13. B. Yang, D. Zhang, W. She, J. Wang, S. Gao, Y. Wang, and K. Wang, *J. Power Sources* 492, 229666 (2021).
14. S.K. Tiwari, S. Sahoo, N. Wang, and A. Huczko, *J. Sci. Adv. Mater. Devices* 5, 10 (2020).
15. R. Kumar, S. Sahoo, E. Joanni, R.K. Singh, R.M. Yadav, R. Kumar, D.P. Singh, W.K. Tan, A. Pérez, and S.A. Moshkalev, *Nano Res.* 12, 35 (2019).
16. K. Cendrowski, W. Kuku, and E. Mijowska, *Mater. Res. Bull.* 146, 111620 (2022).

17. Z. Husain, S.R.A.R.K.B. Ansari, A.B. Pandit, M.S. Khan, M.A. Qyyum, and S.S. Lam, *Mater. Sci. Energy Technol.* 5, 2022).
18. M. Besir, H. Gürsu, M. Gencten, and Y. Sahin, *J. Energy rage* 35, 102328 (2021).
19. W.-J. Liu, H. Jiang, and H.-Q. Yu, *Energy Environ. Sci.* 1 (2019).
20. H. Shao, Y. Wu, Z. Lin, P. Taberna, P. Simon, H. Shao, Y. Wu, Z. Lin, P. Taberna, and P. Simon, *Chem. Soc. Rev.* 49, 3005 (2020).
21. J. Wang, X. Zhang, Z. Li, Y. Ma, and L. Ma, *J. Power rces* 451, 227794 (2020).
22. L. Luo, T. Chen, Z. Li, Z. Zhang, W. Zhao, and M. Fan, *J. 02 Util.* 25, 89 (2018).
23. H. Chen, Y. Xiong, T. Yu, P. Zhu, X. Yan, Z. Wang, and S. Guan, *Carbon N. Y.* 113, 266 (2017).
24. C. Wang, H. Wang, B. Dang, Z. Wang, X. Shen, C. Li, and Q. Sun, *Renew. Energy* 156, 370 (2020).
25. D. Li, G. Chang, L. Zong, P. Xue, Y. Wang, Y. Xia, C. Lai, and D. Yang, *Energy Storage Mater.* **17**, (2018).
26. Liu, J. Niu, and Z. Zhang, *Nano Energy* 51, 366 (2018).
27. L. Guan, L. Pan, T. Peng, T. Qian, Y. Huang, X. Li, C. Gao, Z. Li, H. Hu, and M. Wu, *Carbon N. Y.* 152, 537 (2019).
28. Y. Ma, X. Zhang, Z. Liang, C. Wang, Y. Sui, B. Zheng, Y. Ye, W. Ma, Q. Zhao, and C. Qin, *Electrochim. Acta* 337, 135800 (2020).
29. Z. Dai, P. Ren, W. He, X. Hou, F. Ren, Q. Zhang, and Y.-L. Jin *Renew. Energy* 162, 613 (2020).
30. L. Luo, L. Luo, J. Deng, T. Chen, G. Du, M. Fan, and W. Zhao, *Int. J. Hydrogen Energy* 46, 31927 (2021).
31. L. Zheng, M. Chen, S. Liang, and Q. Lü, *Diam. Relat. Mater.* 113, 108267 (2021).
32. Y. Xi, J. Cao, J. Li, P. Zhang, Y. Zhu, and W. Han, *J. Energy St e* 37, 102470 (2021).
33. S. Meng, Z. Mo, Z. Li, R. Guo, and N. Liu, *Mater. Chem. Phys.* 246, 122830 (2020).
34. T. Ratnaji and L.J. Kennedy, *Diam. Relat. Mater.* 110, 108100 (2).
35. V. Yang, R.A. Senthil, J. Pan, T.R. Kumar, Y. Sun, and X. Liu, *J. Colloid Interface Sci.* 579, 347 (2020).
36. Z. Liu, Z. Zhou, W. Xiong, and Q. Zhang, *Langmuir* 34, 10389 (2018).
37. L. Zheng, X. Dai, Y. Ouyang, Y. Chen, and X. Wang, *J. rgy Storage* 33, 102152 (2021).
38. T. Wang, Y. Xu, B. Shi, S. Gao, G. Meng, and K. Huang, *React. Funct. Polym.* 143, 104326 (2019).
39. P. Zhou, J. Wan, X. Wang, K. Xu, Y. Gong, and L. Chen, *J. Colloid Interface Sci.* 575, 96 (2020).
40. N. Díez, M. Sevilla, and A.B. Fuertes, *Mater. Today NANO* 16, 100147 (2021).
41. E. Taer, A. Apriwandi, D.R. Andani, and R. Taslim, *J. Mater. Res. Technol.* 15, 1732 (2021).
42. K. Yu, J. Wang, X. Wang, J. Liang, and C. Liang, *Mater. Chem. Phys.* 243, 122644 (2020).
43. avitha, *Int. J. Early Child. Spec. Educ.* 1 597 (2022).
44. M. Martina, J. Jumari, and M. Murningsih, *J. Phys. Conf. Ser.* 1943, 012076 (2021).
45. E. Taer, N. Yanti, W.S. Mustika, A. Apriwandi, R. Taslim, A. Agustino, *Int. J. Energy Res.* 44, 10192 (2020).
46. C. Qin, H. Wang, X. Yuan, T. Xiong, J. Zhang, and J. Zhang, *Chem. Eng. J.* 382, 122977 (2020).
47. S.Y. Foong, R.K. Liew, Y. Yang, Y.W. Cheng, P.N.Y. Yek, W.A.W. Mahari, X.Y. Lee, C.S. Han, D.-V.N. Vo, Q. Van Le, M. Aghbashlo, M. Tabatabaei, C. Sonne, W. Peng, and S.S. Lam, *Chem. Eng. J.* 389, 124401 (2020).
48. A. Apriwandi, E. Taer, R. Farma, R.N. Setiadi, and E. miruddin, *J. Energy Storage* 40, 102823 (2021).
49. E. Taer, Y. Susanti, A. Sugianto, R. Taslim, R.N. Setiadi, S. Bahri Agustino, P. Dewi, and B. Kurniasih, *AIP Conf. Proc.* 1927, 030016 (2018).
50. A. Jain, M. Ghosh, M. Krajewski, S. Kurungot, and M. Michalska, *J. Energy Storage* 34, 102178 (2021).
51. E. Taer, R. Taslim, and A.I.P. Conf, *Proc.* 1927, 020004 (2018).
52. E. Taer, A. Afrianda, R. Taslim, K. Minarni, A. Agustino, A. Apriwandi, and U. Malik, *J. Phys. Conf. Ser.* 1120, 012007 (2018).
53. Z. Ma, H. Liu, and Q. Lü, *J. Energy Storage* 40, 102773 (2021).
54. A. Khan, R.A. Senthil, J. Pan, S. Osman, Y. Sun, and X. Sh *lectrochim. Acta* 335, 135588 (2020).
55. S. Sundriyal, V. Shrivastav, A. Kaur, A. Deep, and S.R. Dhakate, *J. Energy Storage* 41, 103000 (2021).
56. D. Khalafallah, X. Quan, C. Ouyang, and M. Zhi, *Renew. rgy* 170, 60 (2021).
57. O. Boujibar, A. Ghosh, O. Achak, T. Cha, and F. Ghamouss, *J. Energy Storage* 26, 100958 (2019).
58. E. Taer, K. Natalia, A. Apriwandi, R. Taslim, A. Agustino, and R. Farma, *Adv. Nat. Sci. Nanosci. Nanotechnol.* 11, 025007 (2020).
59. E. Taer, M. Deraman, R. Taslim, and A.I.P. Conf, *Proc.* 2013, 33 (2013).
60. Y. Mao, N. Siva, A. Dhar, A. Manjaly, M. Kashif, E.H. Alghurabi, M. Asif, M. Boumaza, Y. Duan, and R.L. Vekariya, *Energy Storage* 40, 102784 (2021).
61. X. Chen, R. Paul, and L. Dai, *Natl. Sci. Rev.* 4, 453 (2017).
62. E. Taer, N. Yanti, and R. Taslim, *J. Mater. Res. Technol.* 19, 1 (2022).
63. C. Ding, T. Liu, X. Yan, L. Huang, S. Ryu, J. Lan, Y. Yu, W. Zhong, and X. Yang, *Nano-Micro Lett.* 12, 1 (2020).
64. E. Taer, A. Apriwandi, A. Agustino, M.R. Dewi, and R. Taslim, *Int. J. Energy Res.* 46, 1467 (2021).
65. Y.L.T. Liu, F. Zhang, and Y. Song, *J. Mater. Chem A* 5, 17705 (2017).
66. D. He, Y. Gao, Z. Wang, Y. Yao, L. Wu, J. Zhang, Z.-H. Huang, and M.-X. Wang, *J. Colloid Interface Sci.* 581, 238 (2020).
67. Z. Ying, Y. Zhang, X. Lin, S. Hui, Y. Wang, Y. Yang, and Y. *Chem. Commun.* 56, 10730 (2020).
68. E. Taer, A. Apriwandi, R. Taslim, and A. Agutino, *J. Mater. . Technol.* 9, 13332 (2020).
69. P.M. Shafi, N. Joseph, A. Thirumurugan, and A.C. Bose, *Chem. Eng. J.* 338, 147 (2018).
70. M. Rafique, S. Hajra, M.Z. Iqbal, G. Nabi, S.S.A. Gillani, and M.B. Tahir, *Int. J. Energy Res.* 45, 4145 (2020).
71. C. Karaman, O. Karaman, N. Atar, and M. Lu, *Phys. Chem. m. Phys.* 23, 12807 (2021).
72. N. Sangtong, T. Chaisuwan, S. Wongkasemjit, H. Ishida, W. Redpradit, K. Seneesrisakul, and U. Thubsuang, *Microp- us Mesoporous Mater.* 326, 111383 (2021).
73. M. Cao, Y. Feng, R. Tian, Q. Chen, J. Chen, M. Jia, and J. Yao, *Carbon N. Y.* 161, 224 (2020
74. R. Farma, M. Deraman, R. Omar, M.M. Ishak, E. Taer, I.A. Talib, and A.I.P. Conf, *Proc.* 1415, 180 (2011).
75. C. Xia, S. Surendran, S. Ji, D. Kim, Y. Chae, J. Kim, M. Je, M. Han, W. Choe, C.H. Choi, H. Choi, J.K. Kim, and U. Sim, *Carbon Energy* 4, 491 (2022).
76. J. Wang, Y. Xu, M. Yan, B. Ren, X. Dong, J. Miao, L. Zhang, X. Zhao, and Z. Liu, *Biomass Bioenerg.* 156, 106301 (2022).
77. Z. Zhang, W. Yang, Y. Wu, G. Yan, L. Li, Y. Qing, and X. Lu, *Ind. Eng. Chem. Res.* 60, 11079 (2021).
78. H. Liu, W. Chen, R. Zhang, C. Xu, X. Huang, H. Peng, and C. Huo, *Appl. Surf. Sci.* 566, 15 2 (2021).
79. M.D. Mehare, A.D. Deshmukh, and S.J. Dhoble, *J. Mater. Sci. Mater. Electron.* 32, 14057 (2021).
80. X. Liang, R. Liu, and X. Wu, *Microporous Mesoporous Mater.* 310, 110659 (2021).
81. M.M. Baig and I.H. Gul, *Biomass Bioenerg.* 144, 105909 2021).
82. M.D. Mehare, A.D. Deshmukh, and S.J. Dhoble, *J. Mater. Sci.* 55, 4213 (2019).

83. S. Sankarnarayanan, M. Hariram, S. Vivekanandhan, and R. Navia, *Energy Storage* 3, e222 (2021).

Novel Solanum torvum Fruit Biomass-Derived Hierarchical Porous Carbon Nanosphere as Excellent Electrode Material for Enhanced Symmetric Supercapacitor Performance

ORIGINALITY REPORT

13%	7%	9%	4%
SIMILARITY INDEX	INTERNET SOURCES	PUBLICATIONS	STUDENT PAPERS

PRIMARY SOURCES

1	Mehmet Bolat, Cenk Yavuz, Mustafa Kaya. "Investigation of dual-functionalized novel carbon supported Sn material from corn stalk for energy storage and fuel cell systems on distributed generations", Journal of Materials Science: Materials in Electronics, 2021 Publication	<1%
2	Submitted to Central University of Rajasthan Student Paper	<1%
3	Submitted to University of California, Merced Student Paper	<1%
4	www.myfoodresearch.com Internet Source	<1%
5	www.physics.ucla.edu Internet Source	<1%
6	academic.oup.com Internet Source	<1%
	aip.scitation.org	

7	Internet Source	<1%
8	dspace.ucuenca.edu.ec Internet Source	<1%
9	Turkan Kopac, Yigit Kırca, Atakan Toprak. "Synthesis and characterization of KOH/boron modified activated carbons from coal and their hydrogen sorption characteristics", International Journal of Hydrogen Energy, 2017 Publication	<1%
10	Submitted to Universidade Estadual de Campinas Student Paper	<1%
11	publications.waset.org Internet Source	<1%
12	Shruti Suriyakumar, Preetam Bhardwaj, Andrews Nirmala Grace, A. Manuel Stephan. "Role of Polymers in Enhancing the Performance of Electrochemical Supercapacitors: A Review", Batteries & Supercaps, 2021 Publication	<1%
13	Submitted to Westlake High School Student Paper	<1%

14	Yunxin Tang, Anuraj Varyambath, Yuanchen Ding, Bailiang Chen, Xinyi Huang, Yu Zhang, Deng-guang Yu, Il Kim, Wenliang Song. "Porous organic polymers for drug delivery: hierarchical pore structures, variable morphologies, and biological properties", Biomaterials Science, 2022 Publication	<1 %
15	cjche.cip.com.cn Internet Source	<1 %
16	ppid.unri.ac.id Internet Source	<1 %
17	mme.wsu.edu Internet Source	<1 %
18	Mikhail Khrizanforov, Ruslan Shekurov, Vasily Miluykov, Leysan Gilmanova et al. "Excellent supercapacitor and sensor performance of robust cobalt phosphinate ferrocenyl organic framework materials achieved by intrinsic redox and structure properties", Dalton Transactions, 2019 Publication	<1 %
19	Zeliang Li, Tingting Chen, Xi Wu, Lu Luo, Zhicheng Zhang, Zhihui Li, Mizi Fan, Zhizhong Su, Weigang Zhao. "Nitrogen-containing high surface area carbon cryogel from co-condensed phenol–urea–formaldehyde resin	<1 %

for CO2 capture", Journal of Porous Materials, 2018
Publication

20	bioflux.com.ro Internet Source	<1%
21	patentimages.storage.googleapis.com Internet Source	<1%
22	rs.figshare.com Internet Source	<1%
23	Submitted to Korea Advanced Institute of Science and Technology Student Paper	<1%
24	Martin Luther Yeboah, Shixue Zhou. "Sand mulch-aided ambient-air fabrication of microporous cocoa waste derived-activated carbon for methylene blue adsorption", International Journal of Environmental Analytical Chemistry, 2022 Publication	<1%
25	Tapan Kumar Behera, Snehalata Pradhan, Priyanka Behera, Pramod Kumar Satapathy, Priyabrata Mohapatra. "A Brief Overview on Facile Synthesis and Challenging Properties of Graphene Nanocomposite: State-of-the-art", Asian Journal of Chemistry, 2022 Publication	<1%

Submitted to Yakın Doğu Üniversitesi

26	Student Paper	<1%
27	Zhang, H.. "Electrochemical properties of ultra-long, aligned, carbon nanotube array electrode in organic electrolyte", Journal of Power Sources, 20071011 Publication	<1%
28	Ghanbari, Kh.. "Preparation of polyaniline nanofibers and their use as a cathode of aqueous rechargeable batteries", Electrochimica Acta, 20061201 Publication	<1%
29	Submitted to Hong Kong University of Science and Technology Student Paper	<1%
30	Megan Enright. "Celebrating Emerging Professionals: The 2023 TMS Young Leader Award Recipients", JOM, 2023 Publication	<1%
31	Submitted to Indian Institute of Science, Bangalore Student Paper	<1%
32	Submitted to Indian Institute of Technology, Kharagpure Student Paper	<1%
33	Submitted to University of Malaya Student Paper	<1%

34	B. Swaraj Kumar, James Varghese, Josephkutty Jacob. "Optimal Thermochemical Material Selection for a Hybrid Thermal Energy Storage System for Low Temperature Applications Using Multi Criteria Optimization Technique", Materials Science for Energy Technologies, 2022 Publication	<1 %
35	P. Muhammed Shafi, Nikhitha Joseph, Raj Karthik, Jae-Jin Shim, A. Chandra Bose, V. Ganesh. "Lemon juice-assisted synthesis of LaMnO3 perovskite nanoparticles for electrochemical detection of dopamine", Microchemical Journal, 2021 Publication	<1 %
36	Poomiwat Phadungbut, Wanida Koo-amornpattana, Pornchai Bumroongsri, Sakhon Ratchahat et al. "Adsorptive purification of CO2/H2 gas mixtures of spent disposable wooden chopstick-derived activated carbon: Optimal synthesis condition", Separation and Purification Technology, 2022 Publication	<1 %
37	Satyanarayana Swamy Vyshnava, Gayathri Pandluru, Kanderi Dileep Kumar, Shiva Prasad Panjala et al. "Biocompatible Ni‐doped CdSe/ZnS semiconductor nanocrystals for	<1 %

cellular imaging and sorting", Luminescence, 2022
Publication

38	Submitted to University of KwaZulu-Natal Student Paper	<1%
39	Ouassim Boujibar, Fouad Ghamouss, Arunabh Ghosh, Ouafae Achak, Tarik Chafik. " Excellent CO capture by ultra ‐ high microporous activated carbon made out from Natural Coal ", Chemical Engineering & Technology, 2020 Publication	<1%
40	Submitted to University of New South Wales Student Paper	<1%
41	sigaa.ufpa.br Internet Source	<1%
42	www.asianpubs.org Internet Source	<1%
43	Submitted to Heriot-Watt University Student Paper	<1%
44	Submitted to Indian Institute of Technology Student Paper	<1%
45	Kijima, M.. "Characterization of porous carbonaceous materials derived from poly(phenylenebutadiynylene)s", Carbon, 200703 Publication	<1%

46	M Martina, J Jumari, M Murningsih. "Phenetic analysis of turkey berry (Solanum torvum Sw.) based on morphological character in Semarang region", Journal of Physics: Conference Series, 2021 Publication	<1 %
47	Rakesh K. Sahoo, Ramesh Kumar Chitumalla, Arya Das, Mamata Mohapatra, Je Moon Yun, Joonkyung Jang, Kwang Ho Kim, Saroj K. Singh. "Scalable Processing Method using Waste Polystyrene to Produce Nitrogen-enriched Porous Carbon for Boosting Supercapacitor Performance", Materials Letters, 2021 Publication	<1 %
48	Submitted to The University of Manchester Student Paper	<1 %
49	Wei-Hao Huang, Duu-Jong Lee, Chihpin Huang. "Modification on biochars for applications: A research update", Bioresource Technology, 2021 Publication	<1 %
50	Xueyang Wang, Fanshu Yuan, Dan Xue, Jie Liu, Jie Wei, Yiwen Wang, Jiahui Wang, Qinghua Qu, Qianli Zhang. " MnO Nanoflowers Decorated on ZIF‐8‐ZnO with Ni Foam Supportfor High‐Performance Supercapacitors ", ChemNanoMat, 2022	<1 %

Publication

51	cqe.ist.utl.pt Internet Source	<1 %
52	d-nb.info Internet Source	<1 %
53	sci-hub.se Internet Source	<1 %
54	www.scilit.net Internet Source	<1 %
55	Guangyu He, Jiajia Ding, Jianguo Zhang, Qingli Hao, Haiqun Chen. " One-Step Ball-Milling Preparation of Highly Photocatalytic Active CoFe O –Reduced Graphene Oxide Heterojunctions For Organic Dye Removal ", Industrial & Engineering Chemistry Research, 2015 Publication	<1 %
56	Shasha Guo, Mukesh Kumar Awasthi, Yuefei Wang, Ping Xu. "Current understanding in conversion and application of tea waste biomass: A review", Bioresource Technology, 2021 Publication	<1 %
57	Submitted to University of Birmingham Student Paper	<1 %
58	hal.umontpellier.fr Internet Source	

		<1 %
59	www.degruyter.com Internet Source	<1 %
60	quieora.ink Internet Source	<1 %
61	Li-Ying Wang, Xue Bai, Yan Wu, Ning Lun, Yong-Xin Qi, Yu-Jun Bai. "Improving the Li-ion storage performance of commercial TiO2 by coating with soft carbon derived from pitch", Electrochimica Acta, 2016 Publication	<1 %
62	cer.ihtm.bg.ac.rs Internet Source	<1 %
63	eprints.unram.ac.id Internet Source	<1 %
64	faculty.ksu.edu.sa Internet Source	<1 %
65	ifory.id Internet Source	<1 %
66	journals.pnu.edu.ua Internet Source	<1 %
67	onlinelibrary.wiley.com Internet Source	<1 %
	open.library.ubc.ca	

68	Internet Source	<1%
69	repository.ubaya.ac.id Internet Source	<1%
70	Deraman, Mohamad, N.S.M. Nor, N.H. Basri, B.N.M. Dollah, Sepideh Soltaninejad, Rusli Daik, Ramli Omar, Mohd Azman Hashim, and Mohd Amir Radhi Othman. "Graphene and Activated Carbon Based Supercapacitor Electrodes", Advanced Materials Research, 2015. Publication	<1%
71	Erman Taer, Rika Taslim. "Brief review: Preparation techniques of biomass based activated carbon monolith electrode for supercapacitor applications", AIP Publishing, 2018 Publication	<1%
72	Hongsheng Yang, Zengling Li, Guoqiang Sun, Xuting Jin, Bing Lu, Panpan Zhang, Tengyu Lin, Liangti Qu. "Superplastic Air‐Dryable Graphene Hydrogels for Wet‐Press Assembly of Ultrastrong Superelastic Aerogels with Infinite Macroscale", Advanced Functional Materials, 2019 Publication	<1%

73	Lakshmanan Karuppasamy, Lakshmanan Gurusamy, Gang-Juan Lee, Jerry J. Wu. "Chapter 1 Synthesis of Metal/Metal Oxide Supported Reduced Graphene Oxide (RGO) for the Applications of Electrocatalysis and Supercapacitors", Springer Science and Business Media LLC, 2019 Publication	<1 %
74	R Taslim, A Agustino, E Taer. "Naturalcarbon-metal composite for supercapacitor application", Journal of Physics: Conference Series, 2018 Publication	<1 %
75	Xingwei Tang, Chengling Zhu, Dongdong Cheng, Han Zhou, Xianghui Liu, Peiwen Xie, Qibin Zhao, Di Zhang, Tongxiang Fan. " Architectured Leaf-Inspired Ni Co S /Graphene Aerogels via 3D Printing for High-Performance Energy Storage ", Advanced Functional Materials, 2018 Publication	<1 %
76	journal.hep.com.cn Internet Source	<1 %
77	Liu, Nianping, Jun Shen, and Dong Liu. "Activated high specific surface area carbon aerogels for EDLCs", Microporous and Mesoporous Materials, 2013. Publication	<1 %

78	Pulok Das, Nirmalya Sankar Das, Kausik Sardar, Brahami Das, Ashadul Adalder, Kalyan Kumar Chattopadhyay. "Morphology tuned electrochemical properties of CuBO2 nanostructures", Materials Chemistry and Physics, 2023 Publication	<1 %
79	T. Navrátil, M. Kopanica. "Analytical Application of Silver Composite Electrode", Critical Reviews in Analytical Chemistry, 2002 Publication	<1 %

Exclude quotes	Off	Exclude matches	Off
Exclude bibliography	Off		